Recent Results From the DIII–D Tokamak*

A.G. Kellman for the DIII–D Team
General Atomics
P.O. Box 85608, San Diego, California 92186-9784

ABSTRACT

The goal of the DIII–D program is to provide the integrated basis for commercially attractive steady state fusion power plants. Significant progress toward this goal has been achieved, enabled by system improvements including an error field correction coil, an expanded diagnostic set, a digital plasma control system, and high power rf systems. Simultaneous improvements in both the confinement and stability have been achieved during both VH–mode and negative central shear discharges. Fully non-inductive discharges with high bootstrap current fraction have been obtained. The divertor program has demonstrated simultaneous reduction of divertor heat flux and effective particle control using gas puffing and an in-vessel cryopump. Control of the wall particle inventory, He exhaust, and characterization of the scrapeoff layer and divertor plasma have been achieved. Progress has also been made in addressing additional specific needs for ITER: investigation of basic transport scaling, disruption characterization and avoidance, material erosion, and steady state beta limits.

I. INTRODUCTION

The goal of the DIII–D program is to develop the physics and technology basis for a commercially attractive steady state fusion power plant. While the typical performance of present day tokamaks appears sufficient to provide ignition in next generation devices, the steady state advanced tokamak concept is aimed at producing more compact, lower cost devices by developing higher fusion power density scenarios. To achieve this, simultaneous improvements in both the confinement and stability are required. In addition, advanced modes of operation must be compatible both with steady state current drive and steady state power and particle handling. Progress toward these goals requires advances both in our understanding and in hardware systems. In this paper, we report on recent results from the DIII–D tokamak relevant to the development of this advanced tokamak concept.

DIII–D is a 2.5:1 aspect ratio device capable of producing a wide range of highly shaped plasma cross sections, including elongation up to 2.6 and triangularity to 1.0 (Fig. 1). Eight neutral beams provide 20 MW of 80 keV deuterium, and 1.5 MW of 110 GHz and 6 MW of 30–120 MHz rf power is available. Plasma current up to 3 MA has been achieved in both limiter and divertor operation.

In the next section, some recent system improvements are described including an error field correction coil, an upgraded digital plasma control system, and commissioning of new high power rf systems. New diagnostics systems are described in the sections on experimental results. In Section III, progress in the understanding and achievement of advanced operating scenarios is described including achievement of high performance negative central shear discharges and the simultaneous achievement of high normalized β ($\beta_N = \beta/(I/aB)$ = 4.9% m-T/MA) and high confinement enhancement factor ($H=\tau_E/\tau_{ITER\text{-}89P}=4$) in VH–mode. In addition, a candidate for an advanced tokamak, the second stable core VH–mode is discussed. In Section IV, results of the divertor research program are discussed. This research is aimed at developing the improved particle control and power exhaust required for both ITER and for higher power density advanced tokamaks. Basic tokamak studies critical to the ITER design are presented in Section V. These include dimensionless scaling studies, disruption studies, material erosion studies, and steady state beta limits for ITER. Section VI describes future upgrades including a highly radiative divertor to reduce the power flow to the divertor plate and high power rf operation for current drive and current profile control.

II. SYSTEM UPGRADES

Non-axisymmetric magnetic error fields resulting from imperfections in the external coil systems have many detrimental effects on tokamak operation. The error field provides a frictional torque on the plasma that destabilizes tearing modes resulting in non-rotating, "locked modes". These modes limit low density operation and often lead to disruptions. It has been shown that the plasma sensitivity to error fields increases with the size of the device[1] so that for ITER, the stable operating space will be significantly restricted unless error fields are extremely low. In order to reduce the error fields in DIII–D, a new coil system has been installed that has the capability of producing fields with either an n = 1, 2, or 3 toroidal mode structure to cancel the existing field asymmetries [2]. The coil system, the "C-coil", consists of six saddle coils installed around the device midplane powered in diametrically opposite pairs using three separate supplies. The phase and amplitude of the applied error field is feedback controlled based on an algorithm that minimizes all the known sources of the m/n = 2/1 error field on DIII–D. The coil is now in routine operation and has significantly increased the stable operating space of DIII–D by reducing the minimum density for the onset of locked modes by factors of two to three (Fig. 1**)** [3]. The C-coil has also proven to be a valuable tool for studying basic tokamak

*Work supported by the U.S. Department of Energy under Contract Nos. DE-AC03-89ER51114. W-7405-ENG-48, DE-FG02-90ER54084, DE-AC05-84OR21400, DE-AC04-94AL85000, DE-FG03-86ER453266, DE-FG03-86ER53225, DE-FG03-93ER81581, and DE-FG03-95ER54294.

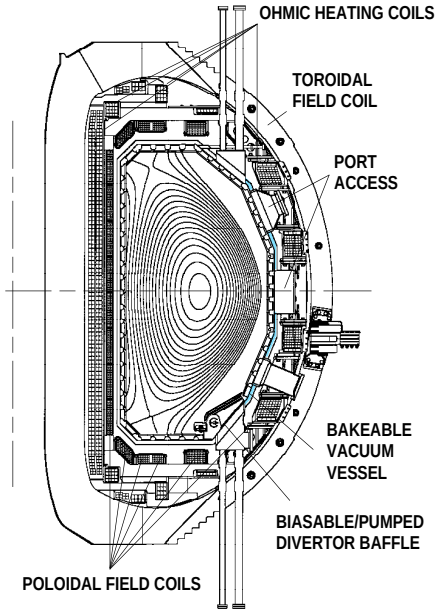

Fig. 1. The cross section of DIII–D with flux surfaces of a double-null divertor discharge superimposed.

transport and stability. Rather than reducing the error field, the mode spectrum of the non-axisymmetric field produced by the coil can be chosen to resonate with different regions of the plasma and the rotation speed can be preferentially reduced in these regions. These "magnetic braking" experiments are described in Section III below.

A key to the success of the DIII–D program has been the highly flexible digital plasma control system [4]. In addition to the control of plasma shape, the system has also been used to control many additional plasma quantities including total stored energy, density, rf loading resistance and radiated power. More recent improvements in the system have included an upgraded control system software that allows simultaneous processing on multiple real time computers, a feature that enables implementation of many of the advanced real-time control algorithms. Some of the new controls that have been added include feedback control of enhanced divertor radiation, neutral pressure, marfe creation, multivariable input-output control of plasma vertical position, and real-time control of safety factor on axis, q(0). Here we briefly describe the integration of the plasma control system with the new MSE diagnostic to measure q(0).

Measurement of the current profile and q profile are essential to the understanding of plasma performance and the implementation of current profile control, a key element in advanced tokamak scenarios. The primary instrument on DIII–D for the measurement of q profiles is the Motional Stark Effect (MSE) diagnostic [57]. This diagnostic makes use of the Stark splitting of the D_α emission from the neutral beam ions to determine the pitch angle of the magnetic field internal to the plasma We currently have 16 channels measuring the magnetic field from just inside the plasma center to the outer plasma edge with a radial resolution from 1.5 to 5 cm and a time resolution of 1 ms. Although the relationship between the full q profile and the magnetic and MSE data is quite complicated, there is a relatively simple expression between the safety factor on axis, the MSE pitch angle measurements, and the plasma elongation on axis, κ_0 [8]. For real time q(0) determination, a fixed value of κ_0 is used based on full MHD equilibrium fits from previous discharges. The real time values of q(0) computed in this manner show excellent agreement with the values determined from full MHD equilibria calculated off-line using all the MSE data. A longer term effort that is being pursued is the real-time solution to the full MHD equilibrium including the q profile across the entire discharge. By combining this ability with rf current drive techniques, complete current profile control can be achieved.

Considerable progress has been made this year in commissioning the higher power rf systems critical to the current drive and current profile modification needs for steady state advanced tokamak scenarios. We are presently operating three FWCD antennas each driven by 2 MW amplifiers (2 MW at 30–60 MHz, 4 MW at 30–80 MHz with decreasing power available up to 120 MHz) for a total power available of 6 MW. A new 1 MW, 110 GHz Russian gyrotron (internal mode convertor) has been tested to full power with a 2 s pulse length.

III. ADVANCED OPERATING REGIMES

Considerable work has been performed in recent years on understanding the various factors that affect confinement and stability in tokamaks. Some of these factors include plasma shape, plasma rotation, wall stabilization, and current profile. In this section we examine these factors and the progress towards combining them to produce a steady state advanced tokamak configuration.

The role of plasma shape was examined in experiments on DIII–D, in which both the elongation, κ, and triangularity, δ, of double-null discharges were independently varied (κ = 1.7 and 2.1 and δ = 0.3 and 0.85). The results showed that the discharge with the highest (κ,δ) had more than twice the fusion product $\beta\tau_E$ (proportional fusion power density) than the lowest (κ,δ) case[9]. Although both shape factors improve performance, it was demonstrated that high triangularity is critical to achieving the high performance.

Plasma rotation near the low order rational q surfaces has also been shown to increase plasma stability by providing wall stabilization of external kink modes in high beta plasmas [10–12]. Detailed measurements of the profile of the plasma safety factor, q, using the new motional Stark effect diagnostic have produced convincing evidence of stabilization by a resistive wall. Beta values 30% greater than the maximum value predicted to be stable against the ideal kink in the absence of an ideal conducting wall have been observed for durations longer than ten wall penetration times. To verify the causal effect of rotation, external magnetic braking using the new C-coil was applied during the high beta phase. When the rotation frequency near the q = 2 and q = 3 surfaces is reduced below approximately 1 kHz, an unstable n = 1 mode is observed to grow and the discharge terminates earlier than without the magnetic braking. These results clearly show that future devices will have to incorporate methods of producing plasma rotation into their designs in order to achieve enhanced stability at high beta.

Strong shear in the toroidal rotation profile was also shown to be a key element responsible for the significant confinement improvement observed in DIII–D Very High confinement (VH–mode) discharges. Comparison of these discharges with normal H–mode indicates that the region where the velocity shear increases most corresponds to the region in which the transport coefficients are reduced the most [13]. Using the C-coil for magnetic braking, the inverse experiments were also performed in which the velocity and velocity shear were reduced and the results showed the causal effect that both turbulence and transport increased in the region of reduced shear [14,15].

The current profile effects on both confinement and stability have been examined on a number of experiments on DIII–D and other devices [16,17]. In DIII–D, record values of normalized β, β_N = 6%-m-T/MA were obtained with peaked current profile, l_i = 2 [18]. Experiments have also indicated that there may be significant benefits to broad current profiles with high edge current. The high confinement observed in VH–modes in JET and DIII–D is correlated to the local access to the second regime of stability to ballooning modes near the edge, afforded by the high edge current density [19]. There is also experimental evidence in DIII–D discharges that q(0) substantially greater than unity is favorable for reducing core transport and improving stability [20,21].

In our investigations of the effect of current profile on plasma performance, we have been examining discharges in which the current profile peaks off-axis in a configuration referred to as reversed, or negative central magnetic shear (NCS). These discharges have negative magnetic shear in the central region of the discharge, where magnetic shear is the rate of change of the average pitch of the magnetic field. Negative central shear allows the plasma to enter the second stable regime for short-wavelength ballooning instabilities and permits the central pressure in the discharge to increase without encountering a beta limit. NCS discharges with very high central pressure, $\beta(0)$ = 44% have been reported in DIII–D [22]. Furthermore, the large pressure gradient in these high performance discharges peaks off-axis producing a non-inductive bootstrap current that is consistent with the profile needed to obtain the negative central shear. Because the high bootstrap current expected in these discharges is consistent with that required to produce the configuration, the rf power required for current drive should be significantly reduced.

In recent experiments we have obtained well documented NCS discharges in both H– and L–mode with high values of β_N (up to 4%-m-T/MA) and H = 3 with with up to 80% non-inductive current drive [23,24]. In these discharges, the negative shear is produce by early injection of neutral beams which slows down the penetration of the current [25] resulting in discharges with central q(0) values $2<q(0)<14$ and minimum values of q $1<q_{min}<3$. The characteristics of these discharges are a highly elevated ion temperature and rotation speed within the central reversed shear region (Fig. 2). Strong peaking of the density profile is also observed in NCS discharges with an L–mode edge. In H–mode discharges with only modest negative central shear, we have obtained β_N = 4%-m-T/MA and H = 3, significantly higher than the values of β_N = 2%-m-T/MA and H = 2 required for the burning plasma phase of ITER. Despite the high rotation speed of these discharges, the high performance phase is typically terminated by a fast growing, low n, MHD event that is initiated by the buildup of edge current density, very similar to the termination of the high performance in VH–mode discharges. These modes are poloidally localized so the wall is not effective at providing stabilization. One solution that we are investigating is NCS discharges with an L–mode edge [26]. In these discharges, the edge pressure gradient has been reduced by more than a factor of ten and the H = 2.5 has been obtained. Record DIII–D performance has been obtained in these discharges with T_i = 22.7 keV, neutron rate of 7.5 x 10^{15} n/s, and central rotation speed of 500 km/s (twice the normal VH–mode rotation speed). These discharges clearly exhibit improved core confinement and ion transport has been reduced significantly.

Although not exhibiting negative central shear, VH–mode discharges with weak central shear have simultaneously exhibited superior performance in the both confinement and stability. A record value of $\beta_N H$ = 19.6 has been obtained with β_N = 4.9%-m-T/MA and H = 4. Record values of the fusion parameter $\beta\tau$ = 3%-s have also been produced in DIII–D by extending VH–mode operation to higher current and lower values of q. This was achieved by early beam injection which slowed the penetration of the current profile (similar to the NCS discharges) resulting in central q above one. This 2 MA discharge had q_{95} = 3.4 with β_N = 3.1%-m-T/MA and H = 3.0.

Fully non-inductive current driven discharges have also been obtained in high performance, high poloidal beta VH–mode discharges. In these discharges, more than 80% of the 600 kA plasma current was driven by the bootstrap current with an additional 340 kA from neutral beam current drive. The

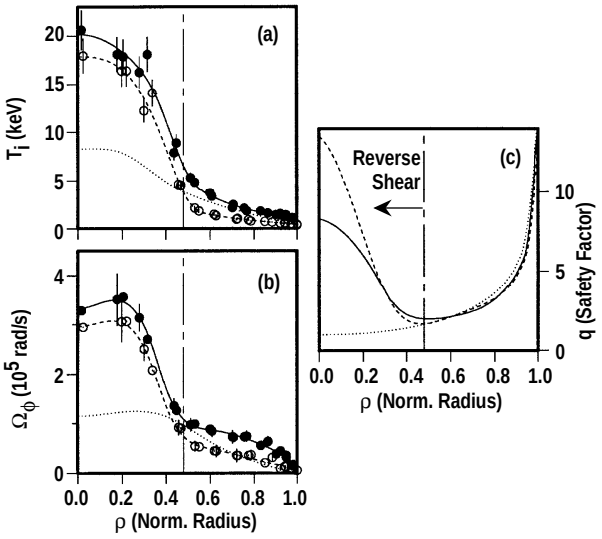

Fig. 2. Measured profiles in L–mode with negative magnetic shear (dash curves and open circles); H–mode with negative magnetic shear (solid curves and solid circles); VH–mode with normal magnetic shear (dotted curves). Profiles include (a) ion temperature, (b) ion toroidal rotation speed, and (c) safety factor. A broken line indicate the maximum radius of shear reversal for the first two cases. For all cases: B = 2.1 T, I = 1.6 MA, P_{NB} = 7.7–8.7 MW.

discharge was maintained at 600 kA by the reverse ohmic drive. We have also demonstrated fully non-inductive current drive using fast waves in the ion cyclotron frequency range (FWCD) in plasmas heated with electron cyclotron resonance heating (ECRH). A plasma current of 170 kA was sustained using 0.8 MW of 60 GHz ECRH and 1.5 MW of FWCD.

These recent experimental results on DIII–D have produced the key elements of advanced tokamak scenarios. By combining many of the features described above, strong plasma shaping, negative or weak central shear, rapid and sheared toroidal rotation profile, broad current profile, and a central q above unity, a clear picture of an advanced tokamak configuration is emerging. Continued development of higher power electron cyclotron and Fast Wave Current Drive systems on DIII–D for current drive and profile control and further advancement of real-time analysis techniques should permit the achievement of our goal of high performance in steady state discharges.

IV. DIVERTOR STUDIES

The objectives of the DIII–D divertor program are twofold. First, to develop and benchmark divertor models for use in designing divertors for future devices by detailed characterization of the scrapeoff layer plasma (SOL). Second, to demonstrate methods of particle control and power handling appropriate for the single null divertor configuration of ITER and the steady state heat load of a high beta, high confinement advanced tokamak. To achieve these goals, we have installed an extensive set of diagnostics on DIII–D and incorporated a biasable toroidal ring, an in-vessel He cryopump and baffles to allow pumping of the lower divertor region.

Recent diagnostic and modeling activities have focused on developing an integrated understanding of the divertor and its relationship to the core and SOL plasma. A 48 channel bolometer array measures radiation along chords that pass through the core and the SOL plasmas and yields emission profiles. Infrared cameras viewing six different locations measure the surface temperature from which the heat flux is derived. Combining these diagnostics into a power balance, we have been able to account for more than 85% of the injected power. Several other diagnostics are used for comparisons with SOL codes and to study the plasma pressure in the SOL. A multichord (36), multi-pulse (seven lasers at 20 Hz each) Thomson scattering system measures n_e and T_e in the core and SOL near the plasma midplane [27]. These data are combined with T_i measurements from an edge Charge Exchange Recombination system to determine the pressure on the midplane and this is compared with the pressure at the divertor floor determined from n_e and T_e measurements from a 20 probe array of Langmuir probes. By using the measured SOL parameters as input to the UEDGE fluid modeling code, we have calculated the heat flux at the divertor strikepoint and a comparison with the infrared measurements shows that the peak heat flux agrees to better than a factor of two and the total agrees within 30% [28].

Recent additions to the diagnostic set have focused particularly on characterizing the divertor plasma. They include a Thomson scattering system for the divertor region, a 250 GHz divertor interferometer, and a movable Langmuir probe. The divertor Thomson system provides n_e and T_e every 50 ms at eight locations from 0–21 cm above the divertor strikeplate [29] . This system has been optimized for the high density and low temperatures expected in this region. Although only recently installed, it has already proved highly reliable and has measured divertor plasmas with density as high as 8×10^{20} m^{-3} and T_e as low as 1.0 eV. The interferometer measures the line density along a chord through the outer divertor leg and by sweeping the X-point, the profile along the field line can be determined. The reciprocating Langmuir probe can be inserted into the X-point region twice during a discharge to measure n_e, T_e, potential, and flow. This diagnostic set will soon be augmented by a broadband UV divertor spectrometer. These new additions to our diagnostic set should significantly improve our ability to characterize the SOL plasma and further develop our divertor modeling ability.

Particle control in DIII–D is provided by an in-vessel He cryopump and baffle structure with a measured pumping speed for D_2 of 30,000 l/s at 2 mTorr. During ELMing H–mode, this pumping system allows the density to be decreased by over 40%, a feature that has allowed us to determine that τ_E scales weakly with n_e and nearly linearly with I_p [30]. Since τ_E does not depend on density, pumping reduces the density and increases T_e which increases the current drive efficiency, a feature that is critical for the success of non-inductive current profile control.

On DIII–D He glow discharge cleaning (HeGDC) is routinely performed between every discharge in order to reduce the particle inventory in the graphite wall and provide the low recycling required for achievement of enhanced confinement H– and VH–modes. A reduction of the net particle inventory in the wall can also be achieved by the use of the cryopump for particle exhaust [31] To demonstrate this, a reference series of ELMing H–mode discharges with HeGDC were performed. This was followed by a sequence of 12 discharges without HeGDC and without active cryopump exhaust, resulting in a net wall loading of 1250 Torr-l (Fig. 3). The cryopump was then activated for the subsequent set of 10 discharges. At the end of this set of discharges the net wall loading was reduced to a value less than the initial wall loading for the reference discharges. In addition, plasma performance during the actively pumped discharges did not suffer without HeGDC as evidenced by the same stored energy in these ELMing H–mode discharges as the reference discharge level. The data suggest that long pulse particle control including the control of the wall inventory can be obtained by divertor pumping alone.

In addition to controlling the plasma density, removal of helium ash is critical for a fusion reactor. Helium pumping has been transiently achieved with a pumping speed of 18,000 l/s by depositing a thin layer of argon on the cryopump. Core He transport and exhaust rates were studied using both He gas puffing from the edge and core He fueling by energetic neutral beams [32,33]. Significant helium exhaust was obtained in a diverted, H–mode plasma with ELMs with the ratio of the effective particle confinement

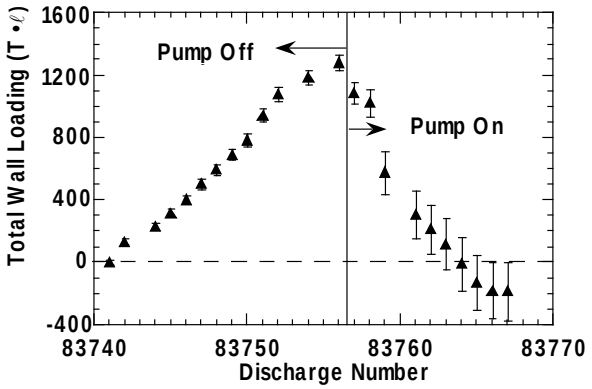

Fig. 3 Cumulative wall loading for the discharges with the cryopump off and on. The He GDC was turned off before the first shot of the sequence and remained off for the entire series of discharges.

time to the energy confinement time, $\tau_{He}/\tau_E \sim 11$, which is within the ITER requirements. There was no evidence of central peaking of the helium density profile even in the presence of this central source. Detailed analysis of the helium profile evolution indicates that the exhaust rate is limited by the exhaust efficiency of the pump (~5%) and not by the intrinsic helium transport properties of the plasmas. Also, perturbative helium transport studies using gas puffing have shown that there is no preferential accumulation of helium in the plasma core in either H– or VH–mode regimes.

One of the major goals of the divertor program is to demonstrate simultaneous reduction of the heat flux to the divertor and particle control. We have previously reported the reduction in the peak heat flux in H–mode plasmas with both D_2, neon, argon, and nitrogen puffing [34,35]. In the D_2 experiments, gas was puffed at 50–150 Torr-l/s either near the plasma midplane or in the divertor, resulting in a decrease in the peak heat flux to the divertor by a factor of 3 to 5. Without pumping, the density usually rises slowly throughout the discharge and there is an increase in radiation from the X-point region [36]. A main feature of the D_2 puffing is a dramatic decrease in the plasma pressure measured at the divertor plate near the separatrix compared to the plasma midplane. This configuration is often referred to as a Partially Detached Divertor (PDD) because the peak divertor heat flux is significantly reduced near the outer strikepoint but the reduction is much less further out in the SOL. Recently, we have added pumping to combine density control with the decrease in the divertor heat flux. We have sustained a PDD discharge with particle exhaust for the full 2 s duration of the D_2 gas puff (Fig. 4) [37]. This was a high quality ELMing H–mode with a confinement factor H ~ 2, with only a very modest decrease in τ_E due to the gas puff, and with a nearly constant density. The core density in these pumped PDD discharges has also been lowered relative to an unpumped case. We have also performed experiments with simultaneous impurity puffing in the divertor, D_2 puffing near the midplane and with pumping. In these discharges the core argon concentration was reduced by a factor of 20 with a midplane D_2 gas flow of 200 Torr-l/s compared to the case without gas flow [35] providing evidence of effective impurity entrainment toward the divertor.

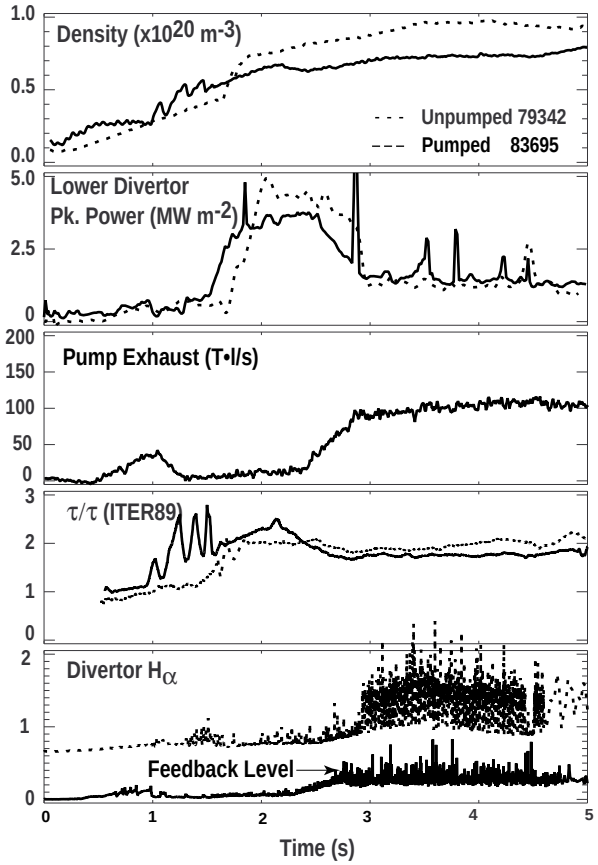

Fig. 4. Effective heat flux reduction to the divertor and particle control have been achieved with D_2 puffing and the use of the cryopump. The pumped (solid) discharge has a lower core density than the unpumped (dash). The gas flow was controlled by the photodiode signal.

V. ITER STUDIES

A major focus of the DIII–D program is to provide critical information to the ITER design group. We report here on some of these ITER relevant studies.

A. *ρ* Scaling Studies*

Recent experiments investigating the underlying transport scaling laws have produced results with significant implication for the ITER design. It has been recognized [38] that present-day tokamaks can operate with all of the dimensionless variables that appear in the basic transport equations (beta, collisionality, safety factor, shape, and machine geometry) at the same values projected for ITER with the exception of the parameter ρ*, the ion gyroradius normalized to the machine size. For ITER, ρ* is significantly smaller than for present devices. By performing experiments on a single machine in which discharges are operated with all dimensionless parameters (except ρ*) held constant and varying ρ*, the basic scaling with ρ* can be determined. This scaling can then be extrapolated to ITER. Earlier experiments on DIII–D and other devices yielded confusing results with the global confinement time varying from Bohm scaling ($\sim\rho^{*0}$) to gyro-Bohm ($\sim\rho^{*1}$). Experiments in L–mode on DIII–D clarified this "discrepancy" by showing that the electrons behave like

gyro-Bohm while the ions behave with Goldston scaling ($\sim\rho^{*-1/2}$), i.e. ion transport increases as either the field or machine size increases [39]. Thus, depending on whether the electrons or ions dominate the energy loss, different experiments can give different results on the transport. Subsequent experiments were performed on DIII–D in H–mode rather than L–mode in which all the key dimensionless variables (other than ρ^*) were the same as for ITER [40]. For these discharges, both the electron and ion transport coefficients scaled like gyro-Bohm ($\sim\rho^{*1}$) as did the global confinement time. This very favorable scaling leads to a confinement enhancement factor of H = 5.3 for ITER. As a result, only 41 MW of input power is required to reach ignition, considerably less than the 300 MW of alpha heating power (Fig. 5). Even counting 70 MW of bremsstrahlung losses, the total power required is much less than the alpha power. These dimensionally similar experiments were performed in H–mode discharges, so it must be shown that at the extrapolated ignition point, ITER will be in H–mode. In Fig. 5, the H–mode power threshold is also plotted, $P_H \propto n^{0.75}BS$ (S is the surface area) and it can be seen that this scales much less favorably with ρ^*, increasing more rapidly than gyro-Bohm for large devices [41]. Similar experiments on JET performed at smaller values of ρ^* more closely tracked the H–mode threshold scaling implying that much higher power levels will be required to reach ignition for ITER unless the H–mode power threshold can be reduced. Comparison of dimensionally identical discharges in DIII–D and C-MOD and DIII–D and JET, are in progress to confirm that the transport is the same for these discharges. Verification of this assumption will provide confidence that this scaling approach can be used to predict the transport behavior on ITER.

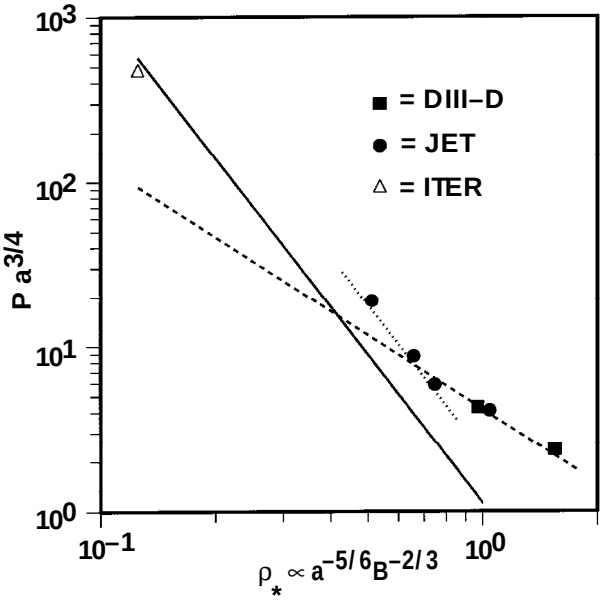

Fig. 5. Loss power versus ρ^* along a dimensionally similar path to ITER. The appropriate dimensionless variables are plotted (constants with dimensions are not shown). The dashed line is a gyro-Bohm extrapolation of the auxiliary heating power based on the DIII–D points only. The solid line is the H–mode power threshold. The dotted line is twice the power threshold.

B. *Disruption studies*

Disruptions and the resulting high heat fluxes and electromagnetic loads on the vessel and internal components are critical issues for ITER and any high current, high power density tokamak. DIII–D has been conducting a series of experiments to fully characterize major disruptions in tokamaks and to provide a good data set to allow development and benchmarking of disruption models. To this end, we have carefully documented impurity induced disruptions, beta limit and density limit disruptions. In these experiments, measurements of density, electron temperature, current profile, scrapeoff layer currents, disruptive heat flux, radiation, fluctuations, and more recently ion temperature and rotation profile have been obtained [42]. Measurements of the ion energy in the divertor during disruptions using DiMES is described in the following section.

In the impurity induced disruption, 2 Torr-l of argon was injected into an H–mode discharge triggering a disruption. The current profile, measured using the MSE system, was observed to broaden rapidly and rather completely. The internal inductance, l_i, dropped from 1.5 to 0.5 in 1.2 ms at the final stage of the thermal quench and the speed of the current profile broadening is faster than can be explained by relaxation due to classical or neoclassical resistive processes. Similarly, strong current profile broadening has been observed in high beta disruptions. Simulations show that the degree of broadening has a major effect on the plasma motion during the disruption. Measurements of n_e and T_e, indicated that most of the energy was lost in 3 to 4 ms as T_e near the center dropped from near 5 keV to approximately 500 eV (Fig. 6). The temperature drops further to ~100 eV by the start of the current decay. During the thermal quench, there is a simultaneous decrease in the core density and an increase in the edge and SOL density resulting in a strong peaking of the density at the plasma edge. In addition, T_e in the SOL increases and the SOL broadens as the core energy decreases. This broadening of the SOL implies that the profile of the heat flux to the divertor plate widens during the thermal quench. Similar behavior is observed in the beta limit disruptions.

We have also begun investigating the toroidal asymmetry of the poloidal or "halo" currents in the scrapeoff layer. These currents can produce large forces on the vacuum vessel and its internal components because they can be a significant fraction of the plasma current (up to 20% in DIII–D) and they interact with the strong toroidal field [43]. An upgraded array of 46 current monitors now permit us to measure both the poloidal and toroidal distribution of these currents. In the impurity induced disruption, a toroidal asymmetry of 1.7:1 (peak-to-average) with an n = 1 distribution is observed in the radiative disruption. The time of the peak coincides with the peak of the current decay rate. Preliminary observation of halo currents in density limit disruptions also indicates significant toroidal asymmetry.

In addition to characterizing disruption phenomenology, we have been working on methods of avoiding disruptions. One promising approach is the use of a neural network to predict the value of beta at which a given discharge will disrupt.

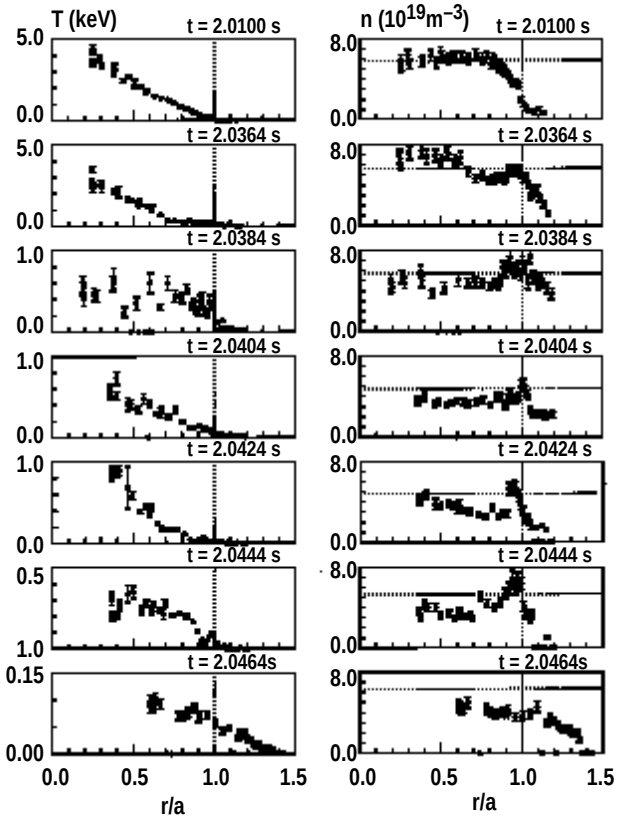

Fig. 6. T_e and n_e profiles versus normalized radius for a disruption induced by argon injection. The plasma edge (separatrix) is shown by the vertical dotted line. The horizontal lines on the density plots are the line average density measured along a midplane radial chord. The thermal quench starts at 2.035 s and ends at 2.045 s. There is a brief reheating period from 2.039 s to 2.044 s.

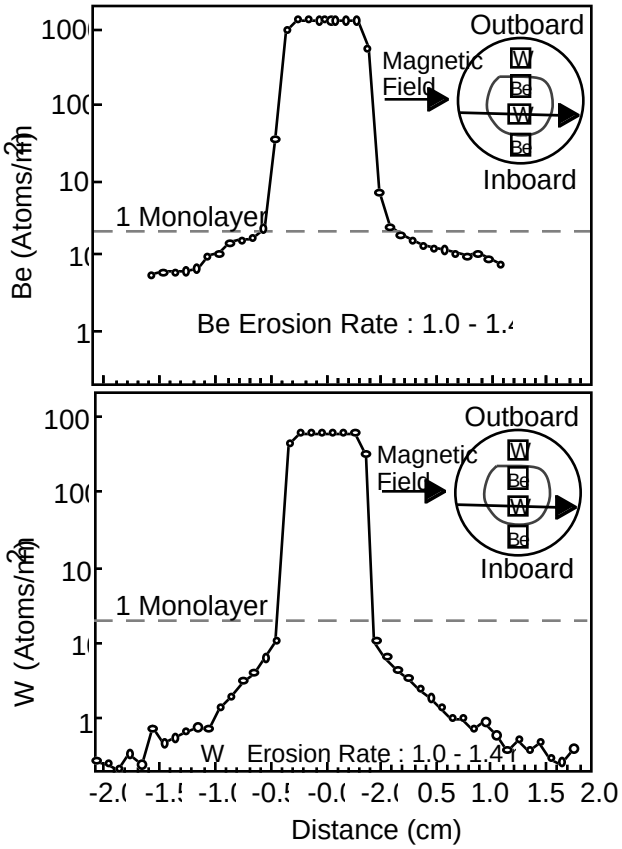

Fig. 7. Areal density profiles for Be and W after exposure to an ELM-free H–mode with a peak heat flux of 0.8 MW/m^2, electron temperature of 70 eV, and magnetic field grazing incidence of 1.5^o.

This real-time generated "beta limit" can then be used in the feedback system to avoid disruptions. Preliminary results are encouraging. The neural network much more accurately predicts the disruption than either of the standard beta limit scaling expressions, $\beta_{max} \sim I/aB$ and $\beta_{max} \sim l_i (I/aB)$. This technique has the potential for providing a real-time system for avoiding or mitigating disruptions in an ignition device. We are now implementing the network into the plasma digital control system to provide a real-time disruption alarm.

C. *DiMES Erosion and Disruption Studies*

A critical need for the design of divertor target materials for ITER is the erosion rate of candidate materials. By allowing insertion of test samples into the DIII–D divertor region, the Divertor Materials Exposure System (DiMES) has been able to provide valuable data on the erosion rates of graphite, tungsten and beryllium. Earlier experiments indicated high erosion rates for graphite and the importance of redeposition in net erosion calculations [44]. Erosion of tungsten was also shown to be 30 times less than for graphite [45]. In more recent experiments, 100 nm thick films of Be and W on a graphite substrate were exposed to heat flux from the outer strike point of a DIII–D ELM-free H–mode. It can be seen in Fig. 7 that Be has a higher net erosion rate (1–1.4 nm/s) and larger redeposition length than tungsten (0.1 nm/s). Although the gross erosion rate of Be is expected to be higher than that for graphite, in fact the erosion rate of the surrounding graphite (3.5 nm/s) is greater than that for the Be film. Indeed, the rapid erosion of graphite resulted in a 2 nm thick layer of carbon measured on the Be film after exposure. This led us to believe that there is an important synergistic effect due to the carbon atoms being deposited onto the Be film during exposure. This apparent reduction in the erosion rate is seen for tungsten, vanadium, and molybdenum. Modeling efforts are underway to understand this effect quantitatively.

In a separate experiment, the outer strikepoint of a single-null divertor discharge was placed on top of the DiMES sample and a disruption was triggered. The DiMES sample consisted of a silicon water shielded from the divertor plasma by a slotted cover that only allowed charge exchange neutrals to impinge on the silicon. The slots were cut at different angles to examine the angular distribution of the neutrals. By using Rutherford back scattering to measure the neutral D_2 areal density versus angle and low energy recoil spectroscopy to measure the depth profile, it was determine that the charge exchange neutrals have energies of approximately 100 eV and are isotropic during the disruption.

D. *ITER Steady State Beta Limits*

In a recent set of experiments, the steady state beta limit was investigated in low density H–mode discharges that carefully

matched the ITER shape. In a surprising result, this limit was found to be well below that expected and at $q_{95} = 2.7$, the limit was only $\beta_N = 2.0\%$-m-T/MA. Moreover, the limit decreased with increasing q_{95}. These discharges were operated at low density and it was hypothesized that the change in current profile and/or collisionality at this density resulted in the low beta limit. In a followup experiment, stable discharges with normalized beta values in excess of 3.0 were obtained by raising the density near the Greenwald limit. Detailed analysis of these discharges is now in progress.

VI. FUTURE PLANS AND SUMMARY

The next improvement to the DIII–D device will be the installation of a radiative divertor configuration [33,46]. The design is based on many of the results discussed in this paper and has utilized the divertor modeling codes, UEDGE and DEGAS to optimize the baffle shape. Slot type divertor channels will be used to reduce the flow of neutrals back to the plasma, and radiation will be used to dissipate the heat flux before it reaches the divertor target. Three in-vessel cryopumps will be used to provide particle control. The design also provides the capability to change the slot length from 23 cm to 43 cm.

Key to further progress in the advanced tokamak scenarios is the advancement of non-inductive current drive. The present 6 MW Fast Wave Current Drive System will be augmented by 10 MW of ECH power at 110 GHz. This will be provided by 1 MW gyrotrons with pulse lengths varying from 2 s to CW. The ECH power will provide the off-axis current drive to augment the bootstrap current and enhance the effectiveness of the on-axis FWCD by raising the electron temperature and thus the current drive efficiency.

The objective of the DIII–D program to demonstrate a steady 30 s duration, fully non-inductive discharge with high confinement and normalized beta remains the focus of our program. The addition of new diagnostics and device improvements have enabled the improved understanding of underlying processes and the development of validated models and simulation capability for future machine design. Several key factors including shape, rotation and current profile have been examined that affect both confinement and stability and enhanced performance has been obtained in both VH–mode and negative central shear discharges. Improved techniques for particle control and heat flux reduction have been developed and detailed characterization of the SOL and divertor plasma have been performed for model development and validation. With the continued development of the advanced tokamak concept, the installation of the radiative divertor and the progress in current drive techniques, all the key ingredients for achievement of our objective and the development of a commercially attractive steady state tokamak will be in place.

ACKNOWLEDGMENTS

This represents the work of the entire DIII–D Team including scientists, engineers and operations personnel, all of whose efforts are greatly appreciated.

REFERENCES

[1] R.J. La Haye, R. Fitzpatrick, T.C. Hender, A.W. Morris, J.T. Scoville and T.N. Todd, "Need Title," *Phys. Fluids B* **4**, 2098, 1992.
[2] J.I. Robinson and J.T. Scoville, "Development of a new error field correction coil "C-Coil" for DIII–D," this conference.
[3] R.J. La Haye and J.T. Scoville, "Use of an m = 2, n = 1 static error field correction coil "The C-Coil" on DIII–D to avoid disruptive locked modes," in Proc. 22nd Euro. Conf. on Plasma Physics and Controlled Fusion (European Physical Society, Petit-Lancy, Switzerland) in press.
[4] J.R. Ferron, et al., "An advanced plasma control system for the DIII–D tokamak," Proc. of the 14th IEEE/NPSS Symp. on Fusion Engineering, vol. 2, pp. 761–764, 1991.
[5] D. Wroblewski and L.L. Lao, "Polarimetry of motional Stark effect and determination of current profiles in DIII-D," *Rev. Sci. Instrum.* **63,** p. 5140, 1990.
[6] B.W. Rice, D.G. Nilson, and D. Wroblewski, "Motional Stark effect upgrades on DIII-D" *Rev.Sci. Instrum.* **66**, p. 373 1995.
[7] F.M. Levington, "The multichannel motional Stark effect diagnostic on TFTR," *Rev. Sci. Instrum.* **63**, p. 5157, 1992.
[8] M. Walker, et al., "Status of DIII–D plasma control," this conference.
[9] E.A. Lazarus, et al., "Dependence of $\beta \cdot \tau$ on plasma shape in DIII–D," in Proc. of the 20th Euro. Conf. on Plasma Heating (European Physical Society, Petit-Lancy, Switzerland) vol. 17C, Part I, p. 95, 1993.
[10] A. Bondeson and D.J. Ward, "Stabilization of external modes in tokamaks by resistive walls and plasma rotation," *Phys. Rev. Lett.* **72**, p. 2709, 1993.
[11] E.J.Strait, et al., "Wall Stabilization of high beta tokamak discharges in DIII-D," *Phys. Rev. Lett.* **74**, p. 2483, 1995.
[12] T.S. Taylor, et al., "Wall stabilization of high beta plasmas in DIII-D," *Phys. Plasmas* **2**, p. 2390, 1995.
[13] T.H. Osborne, et al., "Recent VH-mode results on DIII-D" *Plasma Physics and Controlled Fusion* **36**, A13, 1994.
[14] K.H. Burrell, et al., "Role of the radial electric field in the transition from L-mode to H-mode to VH-mode in the DIII-D tokamak," *Phys. of Plasmas* **1**, p. 1536, 1994.
[15] R.J. La Haye, et al., "Role of core toroidal rotation shear on the turbulence and transport in the improved confinement regimes on DIII-D," in *Local Transport Studies in Fusion Plasmas*, Proc. of the Varenna Workshop, 1993 (Societa Italiana di Fisica, Bologna) p. 283.
[16] M. Zarnstorff , et al., "Overview of recent TFTR results," *Plasma Phys. and Controlled Nucl. Fusion*, vol. 1, p. 111, (International Atomic Energy Agency, Vienna) 1992 .
[17] L.L. Lao, et al., "Regimes of improved confinement and stability in DIII-D obtained through current profile modifications," *Plasma Phys. and Controlled Nucl. Fusion*, vol. 1, p. 565, (International Atomic Energy Agency, Vienna) 1992.
[18] J.R. Ferron, L.L. Lao, T.S. Taylor, Y.B. Kim, E.J. Strait, D. Wroblewski, "Improved confinement and stability in the DIII-D tokamak obtained through modification of the current profile," *Phys. Fluids B* **5**, p. 2532, 1993.
[19] C.M. Greenfield, et al., "Investigations of VH-mode in DIII-D and JET," *Plasma Phys. and Contr. Fusion* **35**, B263, 1993.
[20] P.A. Politzer, et al., "Evolution of high βp plasmas with improved stability and confinement," *Phys. Plasmas* **1**, p. 1545, 1994.
[21] T.A. Casper, et al., "Fluctuations in high βp plasmas in DIII-D," in Proc. 21st Euro. Conf. on Plasma Physics and Controlled Fusion (European Physical Society, Petit-Lancy, Switzerland) 1994.
[22] E.A. Lazarus, et al., "An optimization of beta in the DIII-D tokamak," *Phys. Fluids B* **4**, p. 3644, 1992.
[23] E.J. Strait, et al., "Enhanced confinement and stability in DIII–D discharges with reversed magnetic shear," unpublished.
[24] M.E. Mauel, et al., "Production and stability of high-beta DIII–D discharges with reversed magnetic shear," in Proc. of the 22nd Euro. Conf. on Plasma Physics and Controlled Fusion (European Physical Society, Petit-Lancy, Switzerland) in press.
[25] B.W. Rice, et al., "The formation and evolution of reverse magnetic shear current profiles on DIII–D," General Atomics Report GA-A22127, August, 1995.
[26] B.W. Rice, et al., "Observations of enhanced core confinement in negative magnetic shear discharges with an L-mode edge on DIII–D," unpublished.
[27] T.N. Carlstrom, et al., "Design and operation of the multipulse Thomson scattering diagnostic on DIII-D," *Rev. Sci. Instrum.* **63**, 4901, 1992.
[28] S.L. Allen, et al., "Recent DIII–D divertor research," in Proc. 22nd Euro. Conf. on Plasma Physics and Controlled Fusion (European Physical Society, Petit-Lancy, Switzerland) in press.
[29] T.N. Carlstrom, J.H. Foote, D.G. Nilson, and B.W. Rice, "Design of the divertor Thomson scattering system on DIII-D," *Rev. Sci. Instrum.* **66**, p. 493, 1995.
[30] D.P. Schissel, M.A. Mahdavi, J.C. DeBoo, and M. Le, "Decoupling the effects of plasma current and plasma density on DIII-D H-mode energy confinement," *Nucl. Fusion* **34**, p. 1994, 1994.

[31] R. Maingi, et al., "Control of wall particle inventory with divertor pumping on DIII–D," in press.
[32] M.R. Wade, et al., "He exhaust studies in H-mode discharges in the DIII-D tokamak using an argon frosted divertor cryopump," *Phys. Rev. Lett.* **74**, p. 2702, 1995.
[33] M.R. Wade, et al., "He transport and exhaust studies in enhanced confinement regimes in DIII-D," *Phys. Plasmas* **2**, p. 2357, 1995.
[34] S.L. Allen, et al., "Development of a radiative divertor for DIII-D," *J. Nucl. Mater.* **220–222**, p. 336, 1995.
[35] M.J. Schaffer, et al., "Impurity reduction during 'Puff and Pump' experiments on DIII–D," in press.
[36] T.W. Petrie, et al., "Radiative divertor experiments in DIII–D with deuterium injection," General Atomics Report GA-A21879, August 1995.
[37] D.N. Hill, et al., "Divertor research on DIII–D tokamak," *Plasma Phys. and Controlled Nucl. Fusion,* (International Atomic Energy Agency, Vienna) 1994.
[38] R.E. Waltz, J.C. DeBoo and M.N.Rosenbluth, "Magnetic field scaling of dimensionally similar tokamak discharges,"*Phys. Rev. Lett.* **65**, p. 2390, 1990 .
[39] C.C. Petty, T.C. Luce, et al., "Gyroradius scaling of electron and ion transport," *Phys. Rev. Lett.* **74**, p. 1763, 1995.
[40] C.C. Petty, T.C. Luce, et al., "Non-dimensional transport scaling in DIII-D: Bohm versus gyro-Bohm resolved," *Phys. Plasmas* **2**, p. 2342, 1995.
[41] T.C. Luce and C.C. Petty, "Experimental determination of the dimensionless scaling parameter of energy transport in tokamaks," in Proc. 22nd Euro. Conf. on Plasma Physics and Controlled Fusion (European Physical Society, Petit-Lancy, Switzerland) in press.
[42] P.L. Taylor, A.G. Kellman, B.W. Rice and D.A. Humphreys, "Experimental measurements of the current, temperature and density profile changes during a disruption in the DIII–D tokamak," unpublished.; "DIII–D disruption experiment results," in Proc. 22nd Euro. Conf. on Plasma Physics and Controlled Fusion (European Physical Society, Petit-Lancy, Switzerland) in press.
[43] E.J. Strait, L.L. Lao, J.L. Luxon, and E.E. Reis, "Observation of poloidal current flow to the vacuum vessel wall during vertical instabilities in the DIII-D tokamak," *Nucl. Fusion* **31**, p. 527, 1991.
[44] T.Q. Hua and J.N. Brooks, "Erosion/redeposition analysis of the DIII-D divertor," *J. Nucl. Mater.* **220–222**, p. 342, 1995.
[45] R. Bastasz, et al., "Measurement of carbon and tungsten erosion/redeposition in the DIII-D divertor," *J. Nucl. Mater.* **220–222**, p. 310, 1995.
[46] J.P. Smith, et al., "Engineering design of a radiative divertor for DIII–D," this conference.

APPENDIX I: DIII–D TEAM

S.L. Allen,[a] P.M. Anderson, S. Attenberger,[b] M.E. Austin,[c] F.W. Baity,[b] D.R. Baker, G. Barber,[b] C.B. Baxi, N.H. Brooks,D. Buchenauer,[d] K.H. Burrell, R.W. Callis, G.L. Campbell, J. Candy,[e] T.N. Carlstrom, E. Carolipio,[f] W.P. Cary, V.S. Chan, Y. Chenglum[g] E. Chin, S.C. Chiu, M.S. Chu, S. Coda,[h] J. Cuthbertson,[e] J.C. DeBoo, J.S. deGrassie, E.J. Doyle,[i] A. Ejiri,[j] R. Ellis,[a] R.G. Evanko, J. Evans,[a] T.E. Evans, M.E. Fenstermacher,[a] W. Ferguson,[a] J.R. Ferron, D.K. Finkenthal,[k] R.K. Fisher, J. Fitzpatrick,[f] C.B. Forest, J. Freeman, R.L. Freeman, X. Garbet,[l] R. Geer,[m] P. Gohil, A.M. Gootgeld, J. Greene, K.L. Greene, C.M. Greenfield, R.J. Groebner, D. Hayden,[n] R.W. Harvey, W.W. Heidbrink,[f] P.A. Henline, D.N. Hill,[a] D.L. Hillis,[b] F.L. Hinton, T.R. Hodapp, D.J. Hoffman,[b] J. Hogan,[b] K.L. Holtrop, M.A. Hollerbach, R-M. Hong, W. Houlberg,[b] A.M. Howald, C.L. Hsieh, D.A. Humphreys, A.W. Hyatt, H. Ikezi, N. Isei,[o] G.L. Jackson, G. Jahns,[p] R.A. James,[a] T.H. Jensen, T. Jernigan,[b] R. Jong,[a] R. Junge, K.M. Keith, A.G. Kellman, D.H. Kellman, R. Khayrutdinov,[q] J. Kim, K.W. Kim,[i] Y. Kim, N.P. Kirkpatrick, C.C. Klepper,[b] K. Kupfer,[r] R.J. La Haye, L.L. Lao, C.J. Lasnier,[a] G.J. Laughon, E.A. Lazarus,[b] V, Lebedev,[e] B. Lee,[e] J.-H. Lee,[e] R. Lee, R. Lehmer,[e] A.W. Leonard, J.A. Leuer, Y-R. Lin-Liu, J.M. Lohr, G. Lu, T.C. Luce, S. Luckhardt,[e] V. Lukash,[q] M.A. Mahdavi, R. Mahtafar,[p] R. Maingi,[b] Y. Martin,[s] J.M. McChesney, W.B. McHarg, R. Mett, M.M. Menon,[b] R.L. Miller, S.M. Miller, P.K. Mioduszewski,[b] T. Mizuuchi,[t] C.P. Moeller, G. Monier,[u] R.A. Moyer,[e] A. Nerem, D. Nilson,[a] M.P. Nilsen, R. O'Neill, L. Owen,[b] R. Patterson, W.A. Peebles,[i] P.l. Petersen, T.W. Petrie, C.C. Petty, D.A. Phelps, R.D. Phelps, W. Phelps, J. Phillips, R.l. Pinsker, P.A. Politzer, M. Porkolab,[h] G.D. Porter,[a] R. Prater, K. Redler, E.E. Reis, M.E. Rensink,[a] C.L. Rettig,[i] T. Rhodes,[i] B.W. Rice,[a] J. Robinson, M. Rosenbluth,[e] D. Rothwell, E. Ruskov,[f] G.T. Sager, O. Sauter,[s] M.J. Schaffer, K.M. Schaubel, D.P. Schissel, J.T. Scoville, R.P. Seraydarian, D.L. Sevier, T.C. Simonen, J.P. Smith, R.T. Snider, J. Squire,[t] G.M. Staebler, B.W. Stallard,[a] R.D. Stambaugh, H. St. John, R.E. Stockdale, E.J. Strait, D.W. Swain,[b] P.L. Taylor, T.S. Taylor, T. Terpstra,[v] D.M. Thomas, M. Thomas, S.I. Thompson, P.A. Thurgood A.D. Turnbull, J. Vanderlann, M.L. Walker, M. Wade,[b] R.E. Waltz, J.G. Watkins,[d] W.P. West, D. Whyte,[w] C.P.C. Wong, R. Wood,[a] and D. Wroblewski[p]

PERMANENT ADDRESS

(a) Lawrence Livermore Natnl Lab., USA
(b) Oak Ridge Natnl Lab., USA
(c) U. of Maryland, USA
(d) Sandia Natnl Labs, USA
(e) U. of California at San Diego, USA
(f) U. of California at Irvine, USA
(g) XIN Southwestern Institute, China
(h) Massachusetts Institute of Technology, USA
(i) U. of California at Los Angeles, USA
(j) Natnl Institute Fusion Studies, Japan
(k) U. of California at Berkeley, USA
(l) Tore Supra
(m) University of Paris, France
(n) U. of Illinois, USA
(o) Japan Atomic Energy Research Institute, Japan
(p) ORINCON, USA
(q) Kurchatov Institute, Russia
(r) ORAU, USA
(s) EPFL, Switzerland
(t) Kyoto U., Japan
(u) Commissariat a'l'energie Atomique, France
(v) Princeton Plasma Physics Laboratory, USA
(w) CCFM, Canada